

Hyperfine Spin-Two ($F = 2$) Atoms in Three-Dimensional Optical Lattices: Phase Diagrams and Phase Transitions

Michiel Snoek¹, Jun Liang Song², and Fei Zhou²

¹*Institute for Theoretical Physics, Valckenierstraat 65, 1018 XE Amsterdam, the Netherlands*

²*Department of Physics and Astronomy, The University of British Columbia, Vancouver, B. C., Canada V6T1Z1*

We consider ultracold matter of spin-2 atoms in optical lattices. We derive an effective Hamiltonian for the studies of spin ordering in Mott states and investigate hyperfine spin correlations. Particularly, we diagonalize the Hamiltonian in an on-site Hilbert space taking into account spin-dependent interactions and exchange between different sites. We obtain phase diagrams and quantum phase transitions between various magnetic phases.

PACS numbers: 03.75.Mn, 37.10.Jk, 67.85.Fg

I. INTRODUCTION

Optically trapped ultracold atoms possess various hyperfine spin degrees of freedom. By trapping spinor atoms in optical lattices, one can explore the physics of hyperfine spin correlated ultracold atomic matter which generally has fantastically rich magnetic properties. It had been pointed out a while ago that cold atoms in optical lattices can be used to simulate correlated physics related to the Bose-Hubbard model [1] and the superfluid-Mott insulator transition; this transition, tuned by optical lattice potential depth, has been observed in recent experiments [2]. For cold atoms with hyperfine spins, additional magnetic transitions in Mott states are possible. For instance, spin-one atoms can have either ferromagnetic interactions, such as for ⁸⁷Rb, or antiferromagnetic interactions, as for ²³Na [3, 4, 5]. As shown before for sodium atoms, a first order phase transition between spin-ordered (nematic) and spin-disordered (spin-singlet) ground state occurs [6, 7, 8, 9, 10] in the Mott insulating state. Magnetic fields or magnetization can further induce spontaneous nematic ordering [11, 12].

Correlated spin-2 atoms have also been studied recently and were suggested to possess even richer phases. Apart from nematic and ferromagnetic phases, a cyclic phase is also proposed [13, 14, 15]. Fascinating fractionalized non-abelian vortex structures have been predicted [16, 17]. For nematic condensates, the accidental degeneracy between nematic states with different symmetries (i.e. uni-axial versus bi-axial) has been shown to be lifted by zero point energies of spin-wave excitations which effectively can be attributed to the mechanism of order-from-disorder [18, 19]. In lattices, interactions between spin-two atoms further give rise to new kinds of spin-ordered to spin-disordered transitions [20]. A new class of quantum coherent dynamics induced by quantum fluctuations of spin waves and tuned by the optical lattice potential depth was also investigated recently [21]. The distinct magnetic correlations in Mott insulating states were not taken into account in early studies of Mott-superfluid transitions of spin-2 atoms [22, 23].

Experimentally, atoms on an $F = 2$ manifold are usually less stable than those on an $F = 1$ manifold when

spin-one multiplets are lower in energy and spin-flip scattering processes lead to quick relaxation of $F = 2$ atoms. This is particularly problematic for $F = 2$ multiplets of ²³Na where spin-flip scattering is quite strong. But for ⁸⁷Rb, spin-flip scattering is relatively weak. This isotope is therefore a more likely candidate for observance of the physics of correlated spin-two atoms. Early measurements [24] and theoretical calculations of scattering lengths [25] suggest that spin-2 ⁸⁷Rb atoms have a nematic ground state. Coherent spin dynamics in condensates of spin-one or spin-two cold atoms as well as few-body controlled collisions have already been studied in experiments [26, 27, 28, 29], although direct evidence of spin correlated ultra cold matter in optical lattices is still absent. Investigation of cold atoms with high spins in optical lattices will lead to better understanding of fundamental principles of quantum magnetism; in addition, it might also lead to potential applications towards quantum information storing and processing [30, 31].

In this article, we present detailed analysis of quantum states of spin-2 atoms in optical lattices. This subject was also addressed in a previous work where the authors minimized the mean-field energies of maximally ordered states with respect to a tensor order parameter [20]; those trial wavefunctions approximate the ground states quite well in the limit of large exchange coupling but deviations from those states can be substantial in the intermediate coupling regime. To address all possible ordered phases, in this article we extend our analysis to all possible mean-field states and carry out a systematic calculation to further determine the phase boundaries and the order of the phase transitions. We also discuss quadratic Zeeman effects.

The organization of this paper is as follows. In Section II we define the system and operator-algebra. In Section III we consider the limit of zero hopping and derive exact phase diagrams for arbitrary numbers of atoms per lattice site. In Section IV we describe the self-consistent mean-field technique to deal with nonzero exchange coupling. In Section V we do calculations for nonzero exchange between the sites using this mean-field method for two, three and four particles per site. We conclude our studies in Section VI.

II. DESCRIPTION OF THE SYSTEM

In this section we introduce the theoretical framework to deal with cold gases of $F = 2$ atoms. We describe the algebra of the number and spin operators and derive the Hamiltonian.

A. Algebra

As a starting point we take the usual creation and annihilation operators for $F = 2, m = -2, \dots, 2$ particles:

$$\hat{\psi}_m, \quad \hat{\psi}_m^\dagger, \quad [\hat{\psi}_m, \hat{\psi}_{m'}^\dagger] = \delta_{mm'}. \quad (1)$$

To work conveniently with the hopping term in the Hamiltonian we now introduce another basis. Using the spherical harmonics $Y_{2m}(\theta, \phi)$, the following operators are constructed:

$$\hat{\psi}_{xx} = \frac{1}{\sqrt{2}}(\hat{\psi}_{-2} + \hat{\psi}_2) - \frac{1}{\sqrt{3}}\hat{\psi}_0, \quad (2)$$

$$\hat{\psi}_{yy} = -\frac{1}{\sqrt{2}}(\hat{\psi}_{-2} + \hat{\psi}_2) - \frac{1}{\sqrt{3}}\hat{\psi}_0, \quad (3)$$

$$\hat{\psi}_{zz} = \frac{2}{\sqrt{3}}\hat{\psi}_0, \quad (4)$$

$$\hat{\psi}_{xy} = \frac{i}{\sqrt{2}}(\hat{\psi}_{-2} - \hat{\psi}_2) \quad (5)$$

$$\hat{\psi}_{xz} = \frac{1}{\sqrt{2}}(\hat{\psi}_{-1} - \hat{\psi}_1) \quad (6)$$

$$\hat{\psi}_{yz} = -\frac{i}{\sqrt{2}}(\hat{\psi}_{-1} + \hat{\psi}_1), \quad (7)$$

and the creation operators in the same way. These operators have the following properties [20]:

$$[\hat{\psi}_{\alpha\beta}, \hat{\psi}_{\alpha'\beta'}^\dagger] = \delta_{\alpha\alpha'}\delta_{\beta\beta'} + \delta_{\alpha\beta'}\delta_{\beta\alpha'} - \frac{2}{3}\delta_{\alpha\beta}\delta_{\alpha'\beta'} \quad (8)$$

$$\text{Tr}[\hat{\psi}] = \sum_{\alpha} \hat{\psi}_{\alpha\alpha} = 0. \quad (9)$$

This last property puts a constraint on the constructions of linear operators. For operators

$$\text{Tr}[\Delta\hat{\psi}] = \sum_{\alpha,\beta} \Delta_{\alpha\beta}\hat{\psi}_{\beta\alpha}, \quad (10)$$

the tensor Δ can be always reduced to a traceless one, i.e.,

$$\text{Tr}[\Delta] = \sum_{\alpha} \Delta_{\alpha\alpha} = 0. \quad (11)$$

This constraint is needed, because when introducing this new basis we have enlarged the Hilbert space by constructing six operators out of five. This constraint brings the size of the physical Hilbert space back to the original one.

The density operator in terms of the new operators can be derived as:

$$\hat{\rho} = \sum_m \hat{\psi}_m^\dagger \hat{\psi}_m = \frac{1}{2} \text{Tr}[\hat{\psi}^\dagger \hat{\psi}] = \frac{1}{2} \sum_{\alpha,\beta} \hat{\psi}_{\alpha\beta}^\dagger \hat{\psi}_{\beta\alpha}. \quad (12)$$

The factor $\frac{1}{2}$ appears here because the trace involves a double sum over the operator $\hat{\psi}_{\alpha\beta}$. This same factor will appear later when deriving the hopping term in the Hamiltonian.

The spin operator is straightforwardly derived as:

$$\hat{F}_\alpha = -i\epsilon_{\alpha\beta\gamma}\hat{\psi}_{\beta\eta}^\dagger \hat{\psi}_{\eta\gamma}. \quad (13)$$

It has the following properties:

$$[\hat{F}_\alpha, \hat{F}_\beta] = i\epsilon_{\alpha\beta\gamma}\hat{F}_\gamma, \quad (14)$$

$$[\hat{F}_\alpha, \hat{\rho}] = 0 \quad (15)$$

$$[\hat{F}_\alpha, \text{Tr}[(\hat{\psi}^\dagger)^n]] = 0. \quad (16)$$

The total spin operator is then given by:

$$\hat{F}^2 = \hat{F}_\alpha \hat{F}_\alpha \quad (17)$$

$$= \hat{\psi}_{\beta\eta}^\dagger \hat{\psi}_{\eta\gamma} \hat{\psi}_{\gamma\xi}^\dagger \hat{\psi}_{\xi\beta} - \hat{\psi}_{\beta\eta}^\dagger \hat{\psi}_{\eta\gamma} \hat{\psi}_{\beta\xi}^\dagger \hat{\psi}_{\xi\gamma} \quad (18)$$

$$= \hat{\psi}_{\beta\eta}^\dagger \hat{\psi}_{\gamma\xi}^\dagger \hat{\psi}_{\eta\gamma} \hat{\psi}_{\xi\beta} - \hat{\psi}_{\beta\eta}^\dagger \hat{\psi}_{\beta\xi}^\dagger \hat{\psi}_{\eta\gamma} \hat{\psi}_{\xi\gamma} + 6\hat{\rho}. \quad (19)$$

We also introduce the dimer creation operator as:

$$\hat{D}^\dagger = \frac{1}{\sqrt{40}} \text{Tr}[(\hat{\psi}^\dagger)^2], \quad (20)$$

which has the following properties:

$$[\hat{D}, \hat{D}^\dagger] = 1 + \frac{2}{5}\hat{\rho}. \quad (21)$$

This operator creates two particles which together form a spin singlet. In the same way we can construct an operator which creates three particles which together form a singlet. This is called the trimer operator and defined as

$$\hat{T}^\dagger = \frac{1}{\sqrt{140}} \text{Tr}[(\hat{\psi}^\dagger)^3]. \quad (22)$$

Finally we introduce the nematic operator as:

$$\hat{Q}_{\alpha\beta} = \hat{\psi}_{\alpha\eta}^\dagger \hat{\psi}_{\eta\beta} - \frac{1}{3}\delta_{\alpha\beta} \text{Tr}[\hat{\psi}^\dagger \hat{\psi}] = \hat{\psi}_{\alpha\eta}^\dagger \hat{\psi}_{\eta\beta} - \frac{2}{3}\delta_{\alpha\beta}\hat{\rho}. \quad (23)$$

The non-vanishing eigenvalues of this operator indicate the presence of nematic order [10].

B. Hamiltonian

We consider $F = 2$ atoms in an optical lattice. The laser wavelength is λ . This results in a potential $V(\mathbf{r}) = V_0(\sin^2(2\pi x/\lambda) + \sin^2(2\pi y/\lambda) + \sin^2(2\pi z/\lambda))$. We assume that the optical lattice potential is deep enough

such that the lowest band approximation and the tight binding approximation are applicable. The Hamiltonian is then given as [20]:

$$\hat{\mathcal{H}} = \frac{a_L}{2} \sum_i (\hat{\rho}_i^2 - \hat{\rho}_i) + \frac{b_L}{2} \sum_i (\hat{F}_i^2 - 6\hat{\rho}_i) + 5c_L \sum_i \hat{\mathcal{D}}_i^\dagger \hat{\mathcal{D}}_i - t \sum_{\langle ij \rangle} \text{Tr}[\hat{\psi}_i^\dagger \hat{\psi}_j], \quad (24)$$

where i is the site index, $\langle ij \rangle$ means that the sum is over neighboring sites, t is the hopping parameter and the constants a_L , b_L and c_L can be expressed, in terms of atomic mass M , on-site ground state wavefunction $\hat{\psi}_0(\mathbf{x})$ and scattering lengths a_F in the total hyperfine spin $F = 0, 2, 4$ channels, as:

$$a_L = \frac{4\pi\hbar^2(4a_2 + 3a_4)}{7M} \int d^3\mathbf{x} |\hat{\psi}_0(\mathbf{x})|^4 \quad (25)$$

$$b_L = \frac{4\pi\hbar^2(a_4 - a_2)}{7M} \int d^3\mathbf{x} |\hat{\psi}_0(\mathbf{x})|^4 \quad (26)$$

$$c_L = \frac{4\pi\hbar^2(7a_0 - 10a_2 + 3a_4)}{35M} \int d^3\mathbf{x} |\hat{\psi}_0(\mathbf{x})|^4. \quad (27)$$

The hopping amplitude t is given by the overlap integral

$$t = -\frac{1}{2} \int d^3\mathbf{x} \hat{\psi}_0(\mathbf{x}) \left[-\frac{\hbar^2 \nabla^2}{2m} + V(\mathbf{x}) \right] \hat{\psi}(\mathbf{x} + \frac{\lambda}{2} \mathbf{e}_i), \quad (28)$$

where \mathbf{e}_i are the unit-vectors in x , y and z direction. Note the additional factor $\frac{1}{2}$ appearing here. This factor needs to be inserted, because the trace in the hopping term in Eq. (24) involves a double sum over the indices of the creation and annihilation operators $\hat{\psi}_{\alpha\beta}^{(\dagger)}$.

C. Mott Hamiltonian for $\rho > 1$

We now assume that the system is in a Mott state with ρ particles per site. When the number of particles on a lattice site is larger than one (i.e. $\rho > 1$), we assume that the spin splitting in the virtual hopping process can be ignored. This is justified because $a_L \gg b_L, c_L$, such that the density-density interaction dominates. This leads to an effective Mott Hamiltonian

$$\hat{\mathcal{H}}_{\text{Mott}} = \frac{b_L}{2} \sum_i (\hat{F}_i^2 - 6\hat{\rho}_i) + 5c_L \sum_i \hat{\mathcal{D}}_i^\dagger \hat{\mathcal{D}}_i - J_{\text{ex}} \sum_{\langle ij \rangle} \left(\hat{\psi}_{i,\alpha\beta}^\dagger \hat{\psi}_{j,\beta\alpha} \hat{\psi}_{j,\alpha'\beta'} \hat{\psi}_{i,\beta'\alpha'}^\dagger + \text{h.c.} \right), \quad (29)$$

where $J_{\text{ex}} = t^2/a_L$ is the exchange coupling.

In analogy with the spin $F = 1$ case, we now introduce the 'traceless' operator

$$\hat{Q}_{i;\alpha,\beta,\alpha'\beta'}^\dagger = \hat{\psi}_{i,\alpha\beta}^\dagger \hat{\psi}_{i,\alpha'\beta'} - \frac{1}{10} \text{Tr}[\hat{\psi}_i^\dagger \hat{\psi}_i] \left(\delta_{\alpha\alpha'} \delta_{\beta\beta'} + \delta_{\alpha\beta'} \delta_{\beta\alpha'} - \frac{2}{3} \delta_{\alpha\beta} \delta_{\alpha'\beta'} \right). \quad (30)$$

Using the definition of $\hat{\rho}$, we can rewrite:

$$\hat{Q}_{i;\alpha,\beta,\alpha'\beta'}^\dagger = \hat{\psi}_{i,\alpha\beta}^\dagger \hat{\psi}_{i,\alpha'\beta'} - \frac{1}{5} \hat{\rho}_i \left(\delta_{\alpha\alpha'} \delta_{\beta\beta'} + \delta_{\alpha\beta'} \delta_{\beta\alpha'} - \frac{2}{3} \delta_{\alpha\beta} \delta_{\alpha'\beta'} \right). \quad (31)$$

This operator is 'traceless' because

$$\sum_{\alpha,\beta} \hat{Q}_{i;\alpha\beta,\beta,\alpha}^\dagger = 0. \quad (32)$$

It has the property that is symmetric under interchange of α and β and α' and β' and that

$$\hat{Q}_{i;\alpha\beta,\alpha'\beta'} = \hat{Q}_{i;\alpha'\beta',\alpha\beta}^\dagger. \quad (33)$$

In terms of this operator the exchange term (due to virtual hopping processes) in the Hamiltonian can be rewritten as (up to terms which contain the local density and in the Mott state therefore only give rise to an energy shift):

$$\hat{\mathcal{H}}_{\text{ex}} = -J_{\text{ex}} \sum_{\langle ij \rangle} \left(\hat{Q}_{i;\alpha\beta,\alpha'\beta'}^\dagger \hat{Q}_{j;\alpha\beta,\alpha'\beta'} + \text{h.c.} \right). \quad (34)$$

D. Magnetic Fields: Quadratic Zeeman Effect

The presence of a magnetic field leads to linear and quadratic Zeeman effects. The linear Zeeman effect leads to an additional term in the Hamiltonian

$$\hat{\mathcal{H}}_{\text{lin.Z}} = -q_{\text{lin}} \sum_i \mathbf{B} \cdot \hat{\mathbf{F}}_i. \quad (35)$$

For concreteness we take the magnetic field in the z -direction: $\mathbf{B} = B e_z$ and $\hat{\mathcal{H}}_{\text{lin.Z}} = -q_{\text{lin}} B \sum_i \hat{F}_{i,z}$. However, the total Hamiltonian commutes with $\hat{F}_{i,z}$, so that once the system is prepared, the expectation value $\langle \hat{F}_{i,z} \rangle$ will remain the same. In experiments, atoms are usually initially prepared in the $(2, 0)$ -state. This means that in the experimental situation the linear Zeeman effect is irrelevant. Relevant is the quadratic Zeeman effect. It is important to note that the quadratic Zeeman effect gives an energy shift to the individual particles, depending on their spin-state. Writing $\hat{n}_{i,m} = \hat{\psi}_{i,m}^\dagger \hat{\psi}_{i,m}$, $m = -2, \dots, 2$, the Hamiltonian describing the quadratic Zeeman effect is therefore given by:

$$\hat{\mathcal{H}}_{\text{quad.Z}} = q_{\text{quad}} \sum_i (\hat{n}_{i,1} + \hat{n}_{i,-1} + 4(\hat{n}_{i,2} + \hat{n}_{i,-2})). \quad (36)$$

Observing now that

$$\hat{Q}_{i,zz} = -\frac{1}{3}(\hat{n}_{i,1} + \hat{n}_{i,-1}) - \frac{4}{3}(\hat{n}_{i,2} + \hat{n}_{i,-2}) + \frac{2}{3}\hat{\rho}_i \quad (37)$$

we see that we can write:

$$\hat{\mathcal{H}}_{\text{quad.Z}} = -3q_{\text{quad}} \sum_i \hat{Q}_{i,zz}, \quad (38)$$

where we leave out the term involving $\hat{\rho}_i$ because it only gives a constant contribution.

Like in the case of spin-1 bosons [12] we see that this term does not commute with \hat{F}^2 . Therefore the spin-singlet states are unstable with respect to this perturbation and nematic order is induced for infinitesimally small coupling.

III. ON-SITE SPECTRUM

When the tunneling is zero, the sites are decoupled. In this case the full spectrum can be derived for arbitrary (integer) numbers of particles per site [14, 22]. The local operators $\hat{\rho}$, \hat{F}_α , \hat{D} and \hat{D}^\dagger obey the following commutation relations

$$\begin{aligned} [\hat{F}_\alpha, \hat{\rho}] &= 0 \\ [\hat{F}_\alpha, \hat{D}] &= 0 \\ [\hat{F}_\alpha, \hat{D}^\dagger] &= 0 \\ [\hat{F}_\alpha, \hat{F}_\beta] &= i\epsilon_{\alpha\beta\gamma}\hat{F}_\gamma, \\ [\hat{D}, \hat{\rho}] &= 2\hat{D} \\ [\hat{D}^\dagger, \hat{\rho}] &= -2\hat{D}^\dagger \\ [\hat{D}, \hat{D}^\dagger] &= 1 + \frac{2}{5}\hat{\rho} \end{aligned}$$

The spin-operators commute with all other local operators and form a $SU(2)$ -algebra. The density and dimer operators together form a $SU(1, 1)$ -algebra [14]. This can be seen by defining

$$\hat{D}^- = \sqrt{\frac{5}{2}}\hat{D} \quad (39)$$

$$\hat{D}^+ = \sqrt{\frac{5}{2}}\hat{D}^\dagger \quad (40)$$

$$\hat{D}^z = \frac{\hat{\rho}}{2} + \frac{5}{4}. \quad (41)$$

Those operators obey the algebra:

$$[\hat{D}^z, \hat{D}^\pm] = \pm\hat{D}^\pm \quad (42)$$

$$[\hat{D}^+, \hat{D}^-] = -2\hat{D}^z \quad (43)$$

In analogy with the spin-algebra we now define the Casimir operator \hat{D}^2 as

$$\hat{D}^2 = -\frac{1}{2}(\hat{D}^-\hat{D}^+ + \hat{D}^+\hat{D}^-) + \hat{D}^z\hat{D}^z \quad (44)$$

$$= -\frac{5}{2}\hat{D}^\dagger\hat{D} - \left(\frac{5}{4} + \frac{\hat{\rho}}{2}\right) + \left(\frac{5}{4} + \frac{\hat{\rho}}{2}\right)^2. \quad (45)$$

This operator commutes with \hat{D}^\pm and \hat{D}^z and therefore also with \hat{D}^\dagger , \hat{D} and $\hat{\rho}$. Now we consider a state $|\psi_{\min}\rangle$ with ρ_{\min} atoms (i.e. $\hat{\rho}|\psi_{\min}\rangle = \rho_{\min}|\psi_{\min}\rangle$) and $\hat{D}|\psi_0\rangle = 0$. The operator \hat{D} destroys two atoms that

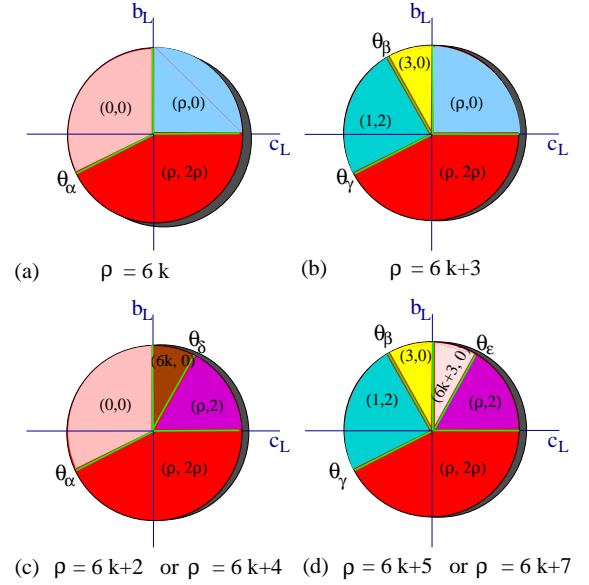


FIG. 1: (Color online) Phase diagrams in the case of isolated lattice sites for various particles numbers ρ . The different phases are indicated by the quantum numbers d and F : (d, F) . The angles $\theta_\alpha, \dots, \theta_\xi$ between the phases depend on the particle number and are defined in the text.

form a singlet pair. That means that the above introduced state $|\psi_{\min}\rangle$ contains no singlet pairs and ρ_{\min} unpaired atoms. Applying \hat{D}^2 to this state we get $\hat{D}^2|\psi_{\min}\rangle = \lambda_D(\lambda_D + 1)|\psi_{\min}\rangle$ with $\lambda_D = \frac{1+2\rho_{\min}}{4}$. Applying now \hat{D}^\dagger to $|\psi_{\min}\rangle$ adds singlet pairs but keeps the number of unpaired atoms constant. Since \hat{D}^2 commutes with \hat{D}^\dagger , all the states $(\hat{D}^\dagger)^n|\psi_{\min}\rangle$ with number of atoms $\rho = \rho_{\min} + 2n_p$ (i.e. ρ_{\min} unpaired atoms and n_p pairs) have the same quantum number $\lambda_D = \frac{1+2\rho_{\min}}{4}$ of the Casimir operator.

So we find a relation between the particle number and the quantum number of the Casimir operator as $\rho = \frac{4\lambda_D - 1}{2} + 2n_p$ which means that for ρ atoms, the possible eigenvalues are $\lambda_D = \frac{2\rho+1}{4} - n_p$, n_p being the number of pairs. We therefore replace the quantum number λ_D by the number of unpaired atoms $d = \rho_{\min} = \frac{4\lambda_D - 1}{2}$.

We can then express the on-site energy in terms of the four quantum numbers ρ , d and F . After some straightforward algebra this yields:

$$\begin{aligned} E(\rho, d, F) &= \frac{a_L}{2}\rho(\rho - 1) + \frac{b_L}{2}(F(F + 1) - 6\rho) \\ &\quad + \frac{c_L}{8}((2\rho + 3)^2 - (2d + 3)^2). \quad (46) \end{aligned}$$

In order to find the ground state, we have to take care of the bosonic symmetry. The requirement that the bosonic wave function is symmetric implies that some combinations of quantum numbers are forbidden. In general for a number of atoms ρ we have $\rho = d + 2n_p$ and $F = 0, \dots, 2d$, because the paired atoms don't contribute to the spin.

However, if $d = 3k$ the values $F = 1, 2, 5, 2d - 1$ are forbidden because of symmetry and if $d = 3k \pm 1$ the values $F = 0, 1, 3, 2d - 1$ are forbidden. By minimizing the energy under those conditions the ground states can be identified. We label each state by two quantum numbers as (d, F) . This yields the phase diagrams as shown in Fig. 1.

The phases are separated by critical angles $\tan \theta = \frac{b_L}{c_L}$, which are given by:

$$\tan \theta_\alpha = \frac{\rho + 3}{4\rho + 2} \quad (47)$$

$$\tan \theta_\beta = -\frac{7}{3} \quad (48)$$

$$\tan \theta_\gamma = \frac{\rho + 4}{4\rho + 6} \quad (49)$$

$$\tan \theta_\delta = 4k + \frac{5}{3} \text{ if } \rho = 6k + 2 \quad (50)$$

$$\tan \theta_\delta = 8k + \frac{14}{3} \text{ if } \rho = 6k + 4 \quad (51)$$

$$\tan \theta_\epsilon = 4k + \frac{11}{3} \text{ if } \rho = 6k + 5 \quad (52)$$

$$\tan \theta_\epsilon = 8k + \frac{26}{3} \text{ if } \rho = 6k + 7 \quad (53)$$

The states appearing in this limit are

- Ferromagnetic: $d = \rho, F = 2d = 2\rho$
- Trimer: $d = \rho = 3k, F = 0$
- Cyclic: $d = \rho = 3k \pm 1, F = 2$
- Dimer: $d = 0, F = 0$
- Nematic: $d = 1, F = 2$.

It is worth remarking that strictly speaking for individual lattice site, there is no long range order and symmetry-breaking states do not exist in this limit. However, infinitesimal hopping could couple the directors of the broken symmetries in some cases and establish long range order; the notations of *nematic* and *cyclic* introduced above refer to states which will have the respective long range order if infinitesimal hopping is allowed and are only truly meaningful when nonzero hopping is taken into account.

In the numerical scheme pursued in the next sections, we distinguish the phases by the following order parameters:

- Ferromagnetic: $\langle \hat{D}^\dagger \hat{D} \rangle = 0, \langle \hat{F}^2 \rangle = 2\rho(2\rho + 1)$.
- Trimer: $\langle \hat{F}^2 \rangle = 0, \langle \hat{D}^\dagger \hat{D} \rangle = 0, \langle \hat{Q}_{\alpha\beta} \rangle = 0$.
- Cyclic: $\langle \hat{D}^\dagger \hat{D} \rangle = 0, 0 < \langle \hat{F}^2 \rangle < 2\rho(2\rho + 1), \langle \hat{Q}_{\alpha\beta} \rangle = 0$.
- Dimer: $\langle \hat{F}^2 \rangle = 0, \langle \hat{D}^\dagger \hat{D} \rangle = \frac{\rho(\rho+3)}{10}, \langle \hat{Q}_{\alpha\beta} \rangle = 0$.
- Nematic: $\langle \hat{F}_\alpha \rangle = 0, \langle \hat{Q}_{\alpha\beta} \rangle \neq 0, \langle \hat{D}^\dagger \hat{D} \rangle > 0$.

IV. NONZERO TUNNELING

We now turn to the case of nonzero tunneling between neighboring lattice sites. In this case there is a competition between states with broken symmetries or long range order and states without broken symmetries. To deal with this situation we make the Ansatz that the total many-body wave function is a product wave function over the lattice sites:

$$|\Psi_{\text{tot}}\rangle = \prod_i |\Psi_i\rangle_i.$$

We moreover assume that the spatial symmetry is unbroken, such that the wavefunctions are identical on each lattice site. We thereby exclude antiferromagnetically ordered states, but they turn out to have higher energy than the states with unstaggered long range order. In the numerical scheme they would moreover be identified by oscillating solutions. Following this procedure the Hamiltonian in Eq. (29) turns into a local Hamiltonian, which is coupled in mean-field to the neighboring lattice sites:

$$\begin{aligned} \hat{\mathcal{H}}_{\text{MF}} = & \frac{b_L}{2} \sum_i (\hat{F}_i^2 - 6\hat{\rho}_i) + 5c_L \sum_i \mathcal{D}_i^\dagger \mathcal{D}_i \\ & - J_{\text{ex}} \sum_{\langle ij \rangle} \left(\hat{Q}_{i;\alpha\beta,\alpha'\beta'}^\dagger Q_{j;\alpha\beta,\alpha'\beta'} + Q_{i;\alpha\beta,\alpha'\beta'}^* \hat{Q}_{j;\alpha\beta,\alpha'\beta'} \right. \\ & \left. - Q_{i;\alpha\beta,\alpha'\beta'}^* Q_{j;\alpha\beta,\alpha'\beta'} + \text{h.c.} \right), \end{aligned} \quad (54)$$

where $Q_{j;\alpha\beta,\alpha'\beta'} = \langle \hat{Q}_{j;\alpha\beta,\alpha'\beta'} \rangle$. The term $J_{\text{ex}} Q_{i;\alpha\beta,\alpha'\beta'}^* Q_{j;\alpha\beta,\alpha'\beta'}$ is a constant term in the Hamiltonian. However, this term is important for comparing energies of the different states, to be able to identify the ground state solution in the case of multiple stable solutions.

Since this is now only a local problem we drop the site index and get (also dropping the constant terms):

$$\begin{aligned} \hat{\mathcal{H}}_{\text{local}} = & \frac{b_L}{2} (\hat{F}^2 - 6\hat{\rho}) + 5c_L \hat{D}^\dagger \hat{D} \\ & - z J_{\text{ex}} \left(\hat{Q}_{\alpha\beta,\alpha'\beta'}^\dagger Q_{\alpha\beta,\alpha'\beta'} + \hat{Q}_{\alpha\beta,\alpha'\beta'} Q_{\alpha\beta,\alpha'\beta'}^* \right). \end{aligned} \quad (55)$$

Here we have introduced the lattice coordination number z , which is equal to $z = 6$ for the three-dimensional cubic lattice.

To take into account the full on-site Hilbert space, we use another basis. Namely, we define five symmetric, traceless tensors Δ_μ , which are orthonormal in the sense that

$$\text{Tr}[\Delta_\mu^* \Delta_\nu] = \delta_{\mu\nu}/2. \quad (56)$$

An explicit example of these are given by:

$$\Delta_1 = \frac{1}{2\sqrt{3}} \begin{pmatrix} 1 & 0 & 0 \\ 0 & 1 & 0 \\ 0 & 0 & -2 \end{pmatrix}, \quad \Delta_2 = \frac{1}{2} \begin{pmatrix} 1 & 0 & 0 \\ 0 & -1 & 0 \\ 0 & 0 & 0 \end{pmatrix} \quad (57)$$

$$\Delta_3 = \frac{1}{2} \begin{pmatrix} 0 & 1 & 0 \\ 1 & 0 & 0 \\ 0 & 0 & 0 \end{pmatrix}, \quad \Delta_4 = \frac{1}{2} \begin{pmatrix} 0 & 0 & 1 \\ 0 & 0 & 0 \\ 1 & 0 & 0 \end{pmatrix} \quad (58)$$

$$\Delta_5 = \frac{1}{2} \begin{pmatrix} 0 & 0 & 0 \\ 0 & 0 & 1 \\ 0 & 1 & 0 \end{pmatrix} \quad (59)$$

This choice is arbitrary, but has the advantage that we can work with purely real matrices. In terms of the original spin-operators we have:

$$\begin{aligned} \text{Tr}[\Delta_1 \hat{\psi}] &= -\hat{\psi}_0 \\ \text{Tr}[\Delta_2 \hat{\psi}] &= \frac{1}{\sqrt{2}} (\hat{\psi}_{-2} + \hat{\psi}_2) \\ \text{Tr}[\Delta_3 \hat{\psi}] &= \frac{i}{\sqrt{2}} (\hat{\psi}_{-2} - \hat{\psi}_2) \\ \text{Tr}[\Delta_4 \hat{\psi}] &= \frac{1}{\sqrt{2}} (\hat{\psi}_{-1} - \hat{\psi}_1) \\ \text{Tr}[\Delta_5 \hat{\psi}] &= -\frac{i}{\sqrt{2}} (\hat{\psi}_{-1} + \hat{\psi}_1) \end{aligned}$$

The on-site trial wave function is

$$\begin{aligned} |\Psi\rangle_i &= \sum_{\mu \dots \sigma} C_{\mu \dots \sigma} |\mu \dots \sigma\rangle \\ |\mu \dots \sigma\rangle &= \prod_{\alpha=\mu, \dots, \sigma} \text{Tr}[\Delta_\alpha \hat{\psi}^\dagger] |0\rangle, \end{aligned} \quad (60)$$

where $C_{\mu \dots \sigma}$ is the amplitude at a particular state $|\mu \dots \sigma\rangle$. After tracing over the traceless tensors Δ_μ , we express the expectation value of the Hamiltonian in Eq. (55) in terms of these amplitudes. By minimizing the energy with respect to $C_{\mu \dots \sigma}$, we obtain the ground states in different parameter regions and the mean-field phase diagrams.

V. PHASE DIAGRAMS FOR NONZERO TUNNELING

In this section we present the results of numerical calculations following the scheme introduced in the previous section. We present result for two, three and four particles per lattice site.

A. $\rho = 2$: Two particles per site

For two particles per site we obtain the phase diagram in Fig. 2. As pointed out before [20], in this case, dimer,

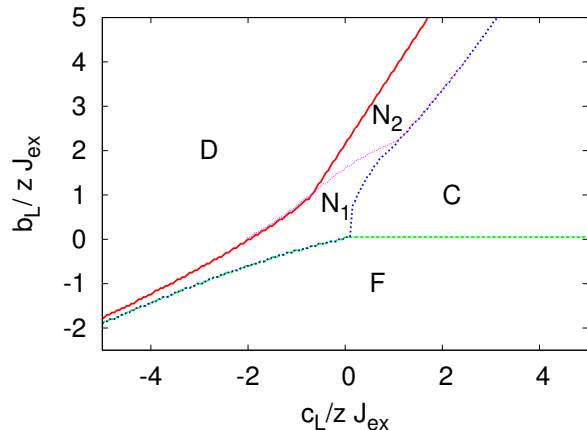


FIG. 2: (Color online) Phase diagram for two particles at a site: phase boundaries between the dimer (D), nematic ($N_{1,2}$), cyclic (C) and ferromagnetic (F) phases

nematic, cyclic and ferromagnetic phases appear. Moreover, we also observe an additional nematic phase between the dimer and cyclic phase; in Fig. 2 this phase is indicated as N_2 . This state differs from the N_1 state by its decomposition in terms of eigenstates of the total spin. The N_1 state has a nonzero projection in the $F = 0$, $F = 2$ and $F = 4$ state, but the N_2 state consists only of states with $F = 0$ and $F = 2$. The $F = 4$ components are absent because of the large value of b_L at the position where this phase appears. We call the N_1 state a Maximally Ordered nematic State and the N_2 state a Minimally Ordered nematic State, because the N_2 state only involves the minimally needed states to break the translational symmetry.

Quantifying the phase diagram we see that for b_L and c_L positive, but when $b_L/c_L < \frac{5}{3}$ the system remains in the cyclic phase. Upon increasing b_L/c_L there is the possibility of a phase transition from the cyclic phase to the nematic phase as J_{ex} is varied and ultimately there is also a transition from the nematic phase to the dimer phase when J_{ex} is decreased. For small J_{ex} the phase boundary between the cyclic and dimer phase approaches $b_L/c_L = 5/3$, in agreement with the analysis in Sec. III. We also find this agreement for the phase boundary between the ferromagnetic and dimer phase: it indeed approaches $b_L/c_L = 1/2$ for small J_{ex} .

In Figs. 3 order parameters are plotted for two ratio's of c_L/b_L . In particular we choose $c_L = 0$ as realized for ^{87}Rb [29] and $c_L/b_L = 0.25$, as realized for ^{23}Na . As is visible there, the N_2 nematic phase experiences a second order transition to the dimer phase. By contrast, the transition between the N_1 nematic phase and the dimer phase as shown in Fig. 3 is of first order. Also the transition between the N_2 nematic phase and the cyclic phase is of first order.

We now investigate the stability of the dimer phase in the presence of a quadratic Zeeman field. The result is

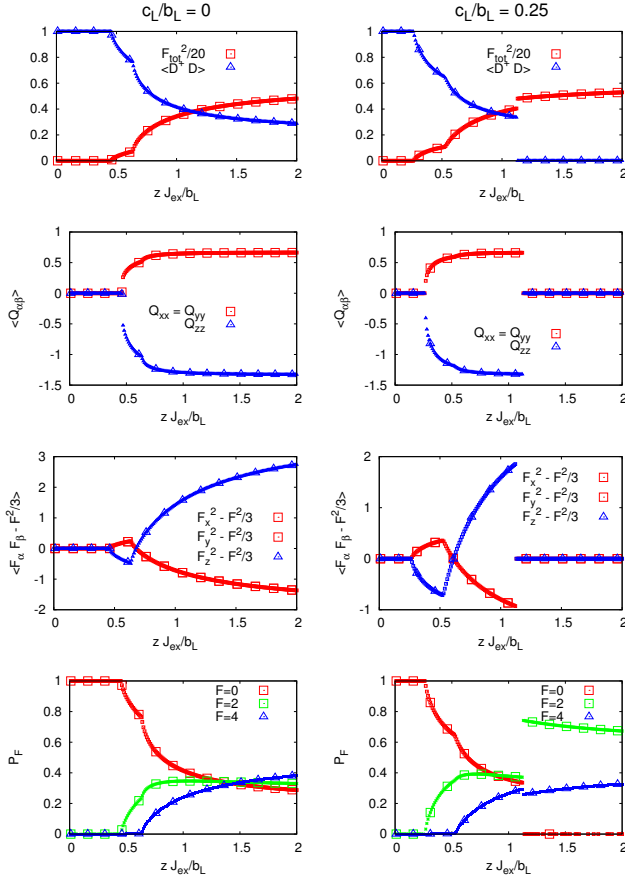


FIG. 3: (Color online) Order parameters for 2 particles per site and two ratios of c_L/b_L . At the top row we plot the expectation value of the dimer counting operator $\hat{D}^\dagger \hat{D}$ and the total spin operator \hat{F}^2 , which is rescaled with a factor 1/20 for visual clarity. The second row displays the eigenvalues of the nematic order parameter $\hat{Q}_{\alpha\beta}$. Two eigenvalues (Q_{xx}, Q_{yy}) are always identical. The third row shows the eigenvalues of the operator $\hat{F}_\alpha \hat{F}_\beta - \frac{1}{3} \delta_{\alpha\beta} \hat{F}^2$. Again, two eigenvalues are identical. At the bottom row we plot the projection of the wave function onto the states with total spin $F = 0, 2, 4$. The total spin states $F = 1, 3$ are not allowed because of the bosonic symmetry. For $c_L/b_L = 0$ (left column) we observe the transition from the dimer phase into the nematic (first N_2 , then N_1) phase. For $c_L/b_L = 0.25$ (right column) the system has an additional transition to the cyclic phase.

presented in Fig. 4. As anticipated, the dimer phase is unstable towards a quadratic Zeeman field and nematic order is induced for infinitesimal couplings.

B. $\rho = 3$: Three particles per site

For three particles per site we obtain the phase diagram in Fig. 5. As predicted before [20] the phase diagram contains the nematic, cyclic, ferromagnetic and trimer phase. Calculating the phase border numerically, we see that the nematic phase extends into the positive c_L

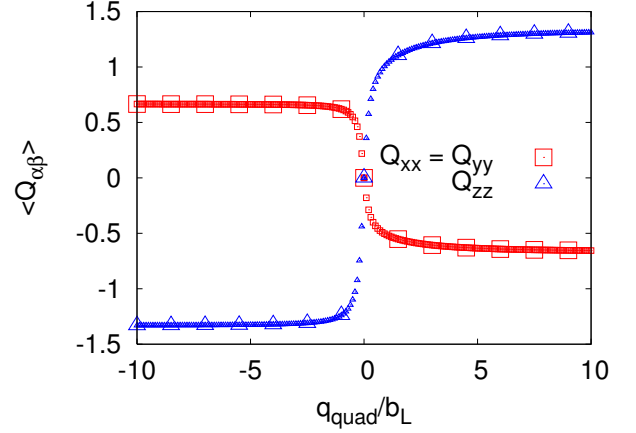


FIG. 4: (Color online) Eigenvalues of the nematic tensor in the presence of a quadratic Zeeman field for two particles per site in the dimer phase ($c_L/b_L = 0$, $z J_{\text{ex}}/b_L = 0.2$) as a function of q_{quad}/b_L . For nonzero q_{quad} the system always displays nematic order.

quarter. In the asymptotic limit of small J_{ex} we recover the results from Sec. III that the critical slope separating the trimer and nematic phase is given by $b_L/c_L = -7/3$ and between the nematic and ferromagnetic phase by $b_L/c_L = 7/18$.

Again we present the order parameters for two ratios of c_L/b_L in Fig. 6. From this we read off that the cyclic-trimer and nematic-trimer transition are both of first order nature.

We also investigate the stability of the trimer phases against a quadratic Zeeman field. As shown in Fig. 7, the trimer phase is unstable against such a field, even for small values.

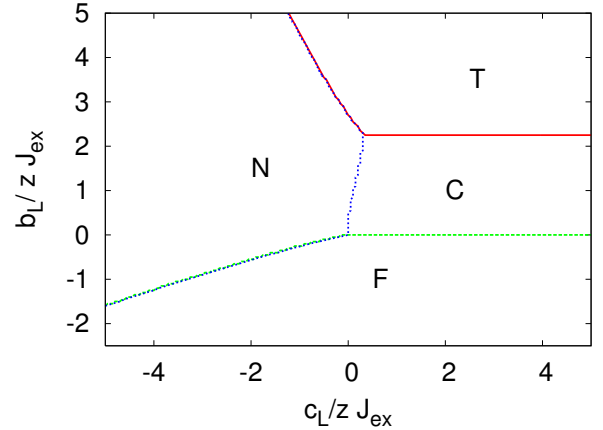


FIG. 5: (Color online) Phase diagram for three particles at a site: phase boundaries between the trimer (T), nematic (N), cyclic (C) and ferromagnetic (F) phases

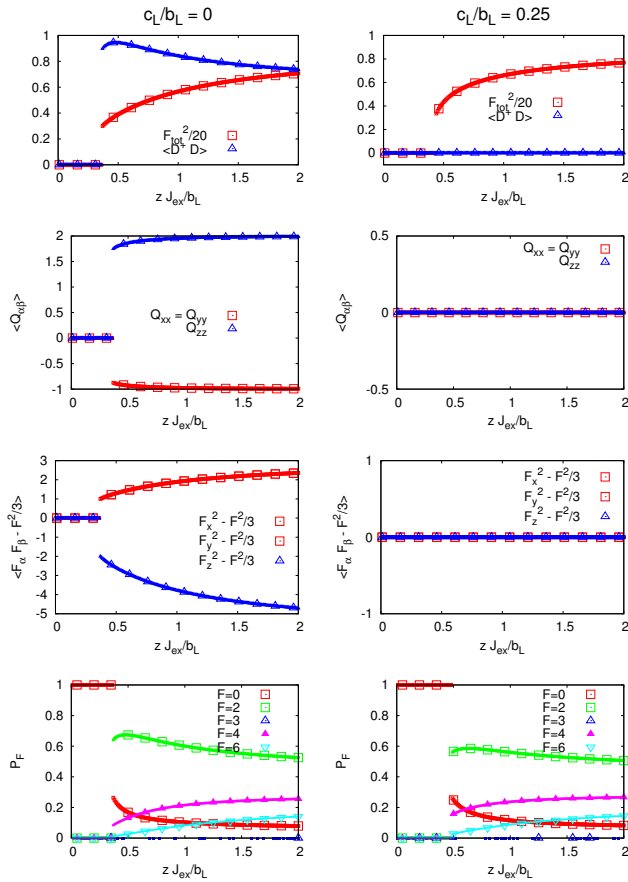


FIG. 6: (Color online) Order parameters for 3 particles per site and two ratio's of c_L/b_L . From top to bottom we plot expectation values of the dimer counting operator $\hat{D}^\dagger \hat{D}$ and the total spin operator \hat{F}^2 , (top row); eigenvalues of the nematic order parameter $\hat{Q}_{\alpha\beta}$ (second row); eigenvalues of the operator $\hat{F}_\alpha \hat{F}_\beta - \frac{1}{3} \delta_{\alpha\beta} \hat{F}^2$ (third row); and the projection of the wave function onto the states with total spin $F = 0, 2, 3, 4, 6$ (bottom row). The total spin states $F = 1, 5$ are not allowed because of the bosonic symmetry. For $c_L/b_L = 0$ (left column) we observe the transition from the trimer phase into the nematic phase. For $c_L/b_L = 0.25$ (right column) the system undergoes the trimer-cyclic transition.

C. $\rho = 4$: Four particles per site

For four particles per site we get the phase diagram in Fig. 8. Like in the case of two particles per site we obtain the ferromagnetic, cyclic, dimer and nematic phase.

Also in this case, the nematic phase is split into two sub-phases. The N_2 phase has only a projection into the $F = 0$ and $F = 2$ states, but the N_1 state has a projection into all the allowed total spin eigenstates. In analogy to the case for $\rho = 2$, we call the N_1 a Maximally Ordered nematic State and the N_2 a Minimally Ordered nematic State. However, in contrast with the case of two particles per site, the nematic phase (N_2) only spreads over a finite area of the parameter space. For large b_L/zJ_{ex}

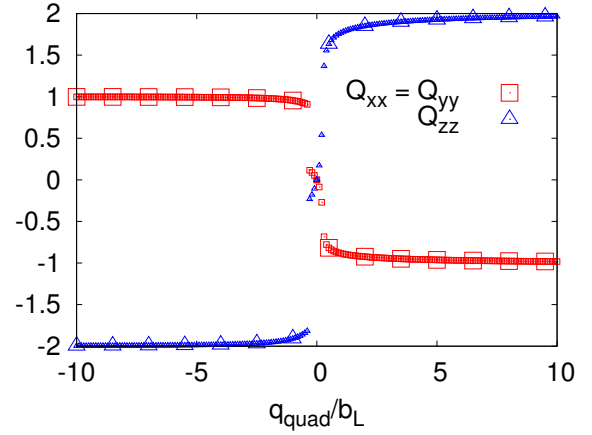


FIG. 7: (Color online) Eigenvalues of the nematic tensor in the presence of a quadratic Zeeman field for three particles per site in the trimer phase ($c_L/b_L = 0$, $zJ_{\text{ex}}/b_L = 0.2$) as a function of q_{quad}/b_L . For nonzero q_{quad} there is always nematic order.

there is a direct transition between the dimer phase and the cyclic phase. For small J_{ex} the slope of the phase border between the dimer and cyclic phase is given by $b_L/c_L = 14/3$, in agreement with the analysis in Sec. III. Likewise the phase border between the ferromagnetic and dimer phase is given by $b_L/c_L = 7/18$ for small J_{ex} . We present the order parameters for various ratio's of c_L/b_L in Fig. 9. It is clear that this gives a first order transition between the N_1 phase and the dimer phase. However, in this case also the transition between the N_2 phase and the dimer phase appears to be of first order.

The stability of the dimer phase in a Quadratic Zeeman field is presented in Fig. 10. The dimer phase is unstable against a quadratic Zeeman field for infinitesimal fields.

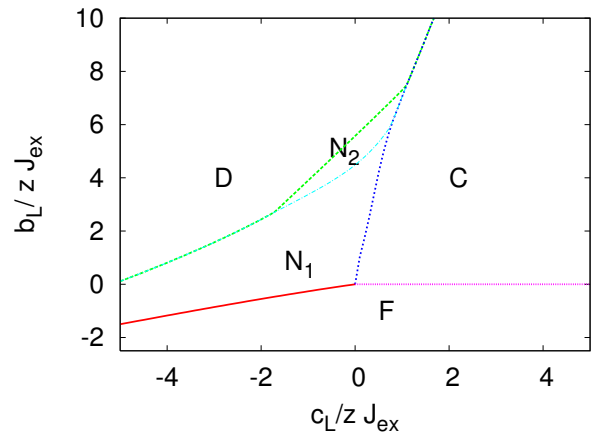


FIG. 8: (Color online) Phase diagram for four particles at a site: phase boundaries between the dimer (D), nematic ($N_{1,2}$), cyclic (C) and ferromagnetic (F) phases

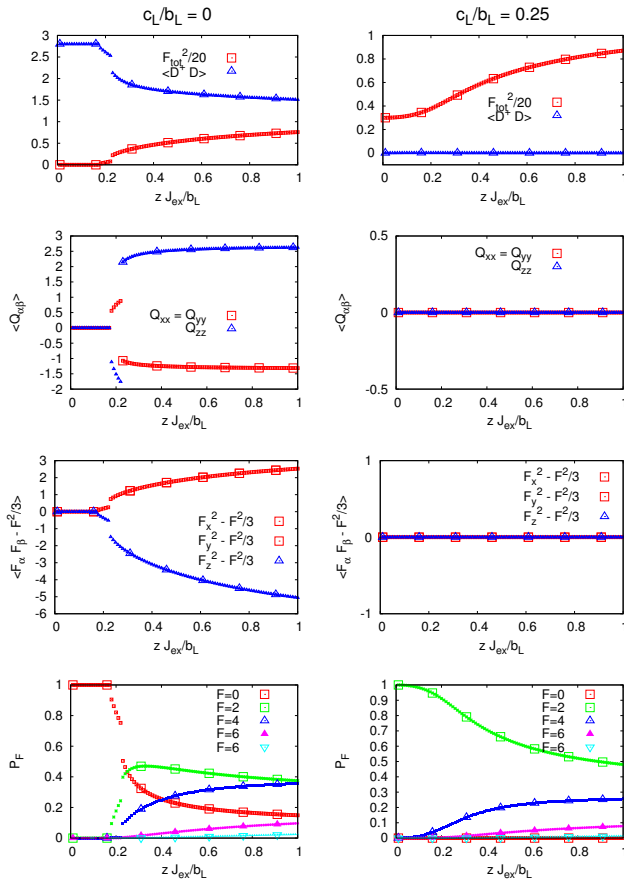


FIG. 9: (Color online) Order parameters for four particles per site and two ratios of c_L/b_L . From top to bottom we plot expectation values of the dimer counting operator $\hat{D}^\dagger \hat{D}$ and the total spin operator \hat{F}^2 (top row); eigenvalues of the nematic order parameter $\hat{Q}_{\alpha\beta}$ (second row); eigenvalues of the operator $\hat{F}_\alpha \hat{F}_\beta - \frac{1}{3} \delta_{\alpha\beta} \hat{F}^2$ (third row); and the projection of the wave function onto the states with total spin $F = 0, 2, 4, 6, 8$ (bottom row). The total spin states $F = 1, 3, 7$ are not allowed because of the bosonic symmetry. Although $F = 5$ is allowed, the states do not have a projection into this total spin state. For $c_L/b_L = 0$ (left column) we observe the transition from the dimer phase into the nematic (first N_2 , then N_1) phase. For $c_L/b_L = 0.25$ (right column) the system is always in the cyclic phase.

D. The case for the $F = 2$ state of ^{87}Rb

We now turn to the experimentally most relevant case of ^{87}Rb . For this case the parameters are such that $c_L = 0$ within experimental accuracy, whereas $a_L/b_L \approx 95$ [29]. It is a particularly important question whether the dimer-nematic and trimer-nematic transitions happen within the Mott regime, i.e. whether on increasing the tunneling amplitude t the transition from the dimer/trimer state occurs before the Mott insulating state is destroyed and the system becomes a superfluid with nematic order.

In order to answer this question we calculate the

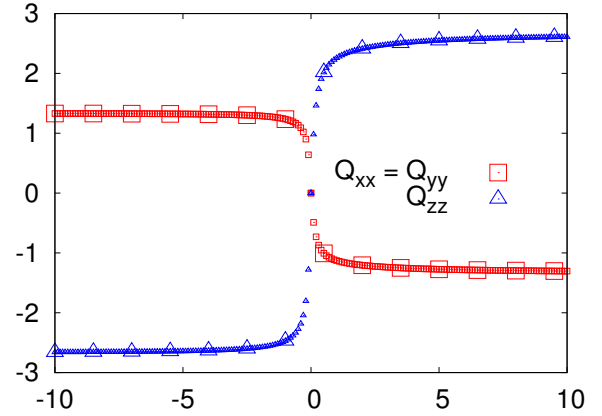


FIG. 10: (Color online) Eigenvalues of the nematic tensor in the presence of a quadratic Zeeman field for four particles per site in the dimer phase ($c_L/b_L = 0$, $z_{J_{ex}}/b_L = 0.1$) as a function of q_{quad}/b_L . For nonzero q_{quad} there is always nematic order.

critical ratio $\frac{b_L}{zJ_{ex}}$ for which the spin-ordered to spin-disordered transition happens. We then estimate the corresponding value of a_L/t and compare it with the critical ratio a_L/t at which the Mott insulator to superfluid transition occurs. We assume a three-dimensional cubic lattice and hence take $z = 6$.

For two particles per site the Mott insulator to superfluid transition for spinless bosons occurs for $a_L/t \approx 100$ (note that t as defined in this paper is half as large as normally used for spinless bosons) [32]. This has to be compared to the value of a_L/t at the dimer-nematic transition, which happens when $\frac{b_L}{zJ_{ex}} \approx 2$ for $\rho = 2$. Taking into account $J_{ex} = \frac{t^2}{a_L}$, we conclude that the dimer-nematic transition happens at $a_L/t \approx 34$ i.e. at a higher value of the hopping amplitude t than the Mott-insulator superfluid transition. This means that for two particles per site the dimer-nematic transition in the Mott phase is preempted by the transition to the superfluid.

For three particles per site the Mott insulator to superfluid transition for spinless bosons occurs for $a_L/t \approx 140$ [32]. This has to be compared to the trimer-nematic transition, which happens for $\frac{b_L}{zJ_{ex}} \approx 2.7$ for $\rho = 3$. This corresponds to $\frac{a_L}{t} \approx 39$. So the trimer-nematic transition won't take place before Mott states enter the superfluid phase

The superfluid-insulator transition for $\rho = 4$ happens at $\frac{a_L}{t} \approx 180$ [32]. As seen from Fig. 6 the dimer-nematic transition occurs for $\frac{b_L}{zJ_{ex}} \approx 5$, which corresponds to $\frac{a_L}{t} \approx 53$. This means that also for four particles per site the dimer-nematic transition is preempted by the Mott-insulator superfluid transition.

However, since the spin-ordering affects the phase boundary to the superfluid phase [22, 23], the precise nature of these transitions remains unclear and further

investigation is needed.

VI. CONCLUSIONS

In this article we studied magnetic transitions in the Mott states of spin-2 atoms for various particle numbers per site. We derived the exact phase diagram for zero tunneling. For the case of nonzero tunneling we used a self-consistent mean-field technique to study the phase diagram. We found various symmetry breaking transitions, depending on the microscopic parameters. In particular, for the microscopic parameters of ^{87}Rb there is the possibility of a dimer-nematic transition and also a transition within the nematic phase, which corresponds to a transition between a maximally ordered

nematic state and a minimally ordered nematic state. However, the nematic-dimer transition happens already for smaller a_L/zJ_{ex} ratio than the usual Mott transition does. Therefore the precise nature of this transition remains to be clarified in future work.

A magnetic field induces a quadratic Zeeman coupling, which within the states with unbroken symmetry gives rise to nematic order even for infinitesimal coupling.

Acknowledgements

This work is supported by the Nederlandse Organisatie voor Wetenschappelijk Onderzoek (NWO) and by NSERC, the Canada and Canadian Institute for Advanced Research

-
- [1] D. Jaksch, C. Bruder, J. I. Cirac, C. W. Gardiner, and P. Zoller, *Phys. Rev. Lett.* **81**, 3108 (1998).
 - [2] M. Greiner, O. Mandel, T. Esslinger, T. W. Hänsch, and I. Bloch, *Nature* **415**, 39 (2002).
 - [3] T. L. Ho, *Phys. Rev. Lett.* **81**, 742(1998).
 - [4] T. Ohmi and K. Machida, *J. Phys. Soc. Jpn.* **67**, 1822 (1998).
 - [5] J. Stenger S. Inouye, D.M. Stamper-Kurn, H.-J. Miesner, A.P. Chikkatur, and W. Ketterle, *Nature* **396**, 345 (1998).
 - [6] E. Demler and F. Zhou, *Phys. Rev. Lett.* **88**, 163001 (2002).
 - [7] F. Zhou, *Europhys. Lett.* **63**, 505 (2003).
 - [8] A. Imambekov, M. Lukin, and E. Demler, *Phys. Rev. A* **68**, 063602 (2003).
 - [9] F. Zhou and M. Snoek, *Ann. Phys. (N.Y.)* **308**, 692 (2003).
 - [10] M. Snoek and F. Zhou, *Phys. Rev. B* **69**, 094410 (2004).
 - [11] A. Imambekov, M. Lukin, and E. Demler, *Phys. Rev. Lett.* **93**, 120405 (2004).
 - [12] F. Zhou, M. Snoek, J. Wiemer, and I. Affleck, *Phys. Rev. B* **70**, 184434 (2004).
 - [13] C. V. Ciobanu, S.-K. Yip, and Tin-Lun Ho, *Phys. Rev. A* **61**, 033607 (2000).
 - [14] Masahito Ueda and Masato Koashi, *Phys. Rev. A* **65**, 063602 (2002).
 - [15] R. Barnett, A. Turner and E. Demler, *Phys. Rev. Lett.* **97**, 180412 (2006).
 - [16] Gordon W. Semenoff and Fei Zhou, *Phys. Rev. Lett.* **98** (2007) 100401.
 - [17] W. V. Pogosov, R. Kawate, T. Mizushima, and K. Machida *Phys. Rev. A* **72**, 063605 (2005).
 - [18] Jun Liang Song, Gordon W. Semenoff, and Fei Zhou, *Phys. Rev. Lett.* **98**, 160408 (2007).
 - [19] Ari Turner, Ryan Barnett, Eugene Demler, Ashvin Vishwanath, *Phys. Rev. Lett.* **98**, 190404 (2007)
 - [20] Fei Zhou and Gordon W. Semenoff, *Phys. Rev. Lett.* **97**, 180411 (2006).
 - [21] Jun Liang Song, Fei Zhou, *Phys. Rev. A* **77**, 033628 (2008).
 - [22] Jing-Min Hou and Mo-Lin Ge, *Phys. Rev. A* **67**, 063607 (2003).
 - [23] Shuo Jin, Jing-Min Hou, Bing-Hao Xie, Li-Jun Tian, and Mo-Lin Ge, *Phys. Rev. A* **70**, 023605 (2004).
 - [24] J.L. Roberts, N.R. Claussen, J.P. Burke, C.H. Greene, E.A. Cornell, and C.E. Wieman, *Phys. Rev. Lett.* **81**, 5109 (1998).
 - [25] N. N. Klausen, J. L. Bohn, and C. H. Greene, *Phys. Rev. A* **64**, 053602 (2001).
 - [26] H. Schmaljohann, M. Erhard, J. Kronjäger, M. Kottke, S. van Staa, L. Cacciapuoti, J. J. Arlt, K. Bongs, and K. Sengstock, *Phys. Rev. Lett.* **92**, 040402 (2004).
 - [27] M.-S. Chang, C. D. Hamley, M. D. Barrett, J. A. Sauer, K. M. Fortier, W. Zhang, L. You, and M. S. Chapman, *Phys. Rev. Lett.* **92**, 140403 (2004).
 - [28] Artur Widera, Fabrice Gerbier, Simon Fölling, Tatjana Gericke, Olaf Mandel, and Immanuel Bloch, *Phys. Rev. Lett.* **95**, 190405 (2005).
 - [29] Artur Widera, Fabrice Gerbier, Simon Foelling, Tatjana Gericke, Olaf Mandel, Immanuel Bloch, *New J. Phys.* **8**, 152 (2006).
 - [30] A. Yu. Kitaev, *Ann. Phys. (N.Y.)* **303**, 2 (2003).
 - [31] R. Raussendorf and H.-J. Briegel, *Phys. Rev. Lett.* **86**, 5188 (2001).
 - [32] F. E. A. dos Santos and A. Pelster, *Phys. Rev. A* **79**, 013614 (2009).